Voltage- and substrate-dependent interactions between sites in putative re-entrant domains of a Na(+)-coupled phosphate cotransporter

Ghezzi, C ; Meinild, A K ; Murer, H ; Forster, I C

Abstract: A common structural feature characterises sodium-coupled inorganic phosphate cotransporters of the SLC34 family (NaPi-IIa/b/c): a pair of inverted regions in the N- and C-terminal halves of the protein. These regions are hypothesised to contain re-entrant domains that associate to allow alternating access of the substrates from either side of the membrane. To investigate if these domains interact during the NaPi-II transport cycle, we introduced novel cysteines at three functionally important sites associated with the predicted re-entrant domains of the flounder NaPi-IIb for the purpose of fluorescent labelling and cross-linking. Single and double mutants were expressed in Xenopus oocytes and their function analysed using electrophysiological and real-time fluorometric assays. The substitution at the cytosolic end of the first re-entrant domain induced a large hyperpolarizing shift in the voltage dependence of steady-state and presteady-state kinetics, whereas the two substitutions at the external face were less critical. By using Cu-phenanthroline to induce disulfide bridge formation, we observed a loss of transport activity that depended on the presence of sodium in the incubation medium. This suggested that external sodium increased the probability of NaPi-IIb occupying a conformation that favours interaction between sites in the re-entrant domains. Furthermore, voltage-dependent fluorescence data supported the hypothesis that a localised interaction between the two domains occurs that depends on the membrane potential and substrate present: we found that the fluorescence intensity reported by a labelled cysteine in one domain was dependent on the side chain substituted at a functionally critical site in the opposed domain.

DOI: https://doi.org/10.1007/s00424-011-0948-z

Pflugers Arch - Eur J Physiol (2011) 461:645–663
DOI 10.1007/s00424-011-0948-z

Voltage- and substrate-dependent interactions between sites in putative re-entrant domains of a Na^+-coupled phosphate cotransporter

Chiara Ghezzi · Anne-Kristine Meinild · Heini Murer · Ian C. Forster

Received: 26 November 2010 / Revised: 7 February 2011 / Accepted: 22 February 2011 / Published online: 8 March 2011

Abstract A common structural feature characterises sodium-coupled inorganic phosphate cotransporters of the SLC34 family (NaPi-IIa/b/c): a pair of inverted regions in the N- and C-terminal halves of the protein. These regions are hypothesised to contain re-entrant domains that associate to allow alternating access of the substrates from either side of the membrane. To investigate if these domains interact during the NaPi-II transport cycle, we introduced novel cysteines at three functionally important sites associated with the predicted re-entrant domains of the flounder NaPi-IIb for the purpose of fluorescent labelling and cross-linking. Single and double mutants were expressed in *Xenopus* oocytes and their function analysed using electrophysiological and real-time fluorometric assays. The substitution at the cytosolic end of the first re-entrant domain induced a large hyperpolarizing shift in the voltage dependence of steady-state and presteady-state kinetics, whereas the two substitutions at the external face were less critical. By using Cu-phenanthroline to induce disulfide bridge formation, we observed a loss of transport activity that depended on the presence of sodium in the incubation medium. This suggested that external sodium increased the probability of NaPi-IIb occupying a conformation that favours interaction between sites in the re-entrant domains. Furthermore, voltage-dependent fluorescence data supported the hypothesis that a localised interaction between the two domains occurs that depends on the membrane potential and substrate present: we found that the fluorescence intensity reported by a labelled cysteine in one domain was dependent on the side chain substituted at a functionally critical site in the opposed domain.

C. Ghezzi · A.-K. Meinild · H. Murer · I. C. Forster (✉)
Institute of Physiology and ZIHP, University of Zurich,
Winterthurerstrasse 190,
CH-8057 Zurich, Switzerland
e-mail: iforster@access.uzh.ch

Keywords Phosphate cotransport · Electrophysiology · Fluorometry · Cross-linking · Voltage dependence · Na^+ cotransporter · Fluorescence · Membrane transport · *Xenopus laevis*

Introduction

Type II sodium/phosphate cotransporters (NaPi-II) belong to a unique class of Na^+-dependent carrier proteins (SLC34A family, according to the Solute Carrier classification: www.bioparadigms.com or 2.1.58/PNAS class, according to the Transporter Classification Database, www.tcdb.org) and show no sequence homology to other known cotransporter families. The family includes three isoforms that can be further classified according to their tissue localisation: the electrogenic NaPi-IIa and electroneutral NaPi-IIc are localised exclusively in the renal proximal tubule and the electrogenic NaPi-IIb is expressed in non-renal epithelial-like tissues [16]. All isoforms share an overall amino acid similarity (≈57%), which is even higher in the predicted transmembrane domain regions [44]; therefore all isoforms most likely share a common 3-D structure. However, the current lack of a crystal structure of bacterial homologs of NaPi-II proteins and the weak sequence homology with other Na-dependent cotransporters, have so far precluded successful homology modelling. It follows that we must use indirect approaches to determine the structure–function relationships of these proteins.

Based on cysteine (Cys) scanning mutagenesis and in vitro transcription/translation assays, a topology model was proposed for NaPi-IIa that is most likely also valid for NaPi-IIb and NaPi-IIc [33]. This model predicts 12 transmembrane-spanning domains (TMDs), with intracellular NH_2 and COOH termini (Fig. 1a). A large extracellular loop between TMDs 5 and 6 links the C- and N-terminal halves of the protein. Analysis of the primary sequence of the three NaPi-II isoforms from different species reveals two regions in each half, 89 residues long, which contain repeated sequences with typically >30% identity (Fig. 1b). Topology predictions indicate that these regions include two TMDs that we have postulated to form re-entrant domains localised between TMDs 2 and 5 and TMDs 7 and 10, respectively [33, 38]. From functional studies using Cys substitutions, we proposed that these putative re-entrant domains may associate to form the P_i transport pathway and, by implication, are also involved in the translocation of the co-substrate (Na^+) in the functionally associated leak mode that operates in the absence of external P_i [3, 20]. However, we still lack evidence of a direct association of the re-entrant domains. For example, the double Cys construct, described in our previous electrophysiology study on the rat NaPi-IIa [20], in which cysteines were substituted in the re-entrant domains, showed a loss of cotransport activity paralleled by a gain in leak activity as Cys modification proceeded. This codetermination of the transport modes by sites in each domain could also have resulted from the Cys substitution in each domain indirectly acting on a structurally separate transport pathway. Furthermore, as that study was performed at a fixed

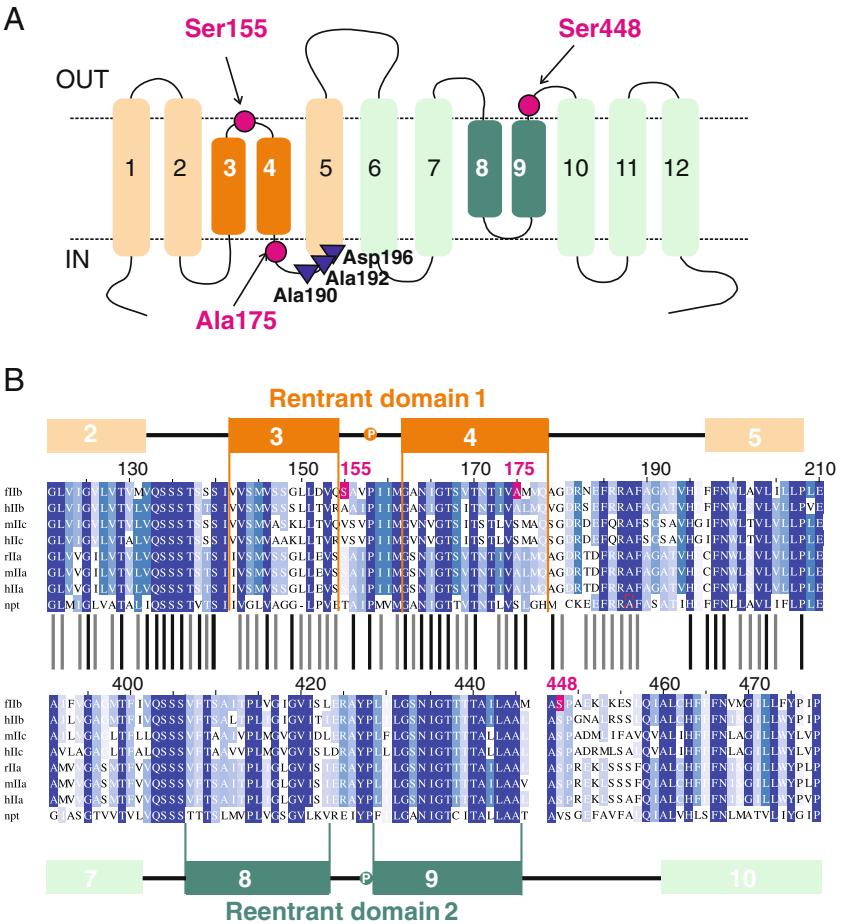

Fig. 1 Re-entrant domains of NaPi-IIb. **a** Topology model of NaPi-II proteins predicts 12 transmembrane domains and intracellular C- and N-termini [33]. Residues that were replaced with a cysteine are indicated as well as three sites at the cytosolic end of TMD5 that are determinants of voltage dependence (see Discussion). *Numbering* is according to flounder NaPi-IIb sequence. **b** Comparison of amino acid sequences from three isoforms of NaPi-IIa/b/c from different species (*fl* flounder, *h* human, *m* mouse, *r* rat) and the bacterial homolog from *Vibrio cholera* (*npt*) using Clustalw [25] for the two repeat regions predicted using the Lalign tool [17]. For flNaPi-IIb, Lalign identifies two regions from the N-terminal and C-terminal halves of the protein with an 89 amino acid overlap that show 31.9% identity. *Vertical bars* indicate identical (*black*) and similar (*grey*) residues in each domain. *Shaded bars* at *top* and *bottom* indicate predicted TMDs (*numbered*). The sites of start and termination of the TMDs were obtained from predictions based on rat NaPi-IIa [33]. A conserved proline is present in the linker regions of each domain, consistent with a putative re-entrant topology. Sites mutated to cysteines in the present study are *coloured magenta* according to the flNaPi-IIb sequence

holding potential of −50 mV the validity of the data was limited to one experimental condition.

Moreover, recent voltage clamp fluorometry (VCF) studies on mutant constructs offer compelling evidence that the parts of the NaPi-II protein associated with the opposed re-entrant domains may move in a complementary manner during the transport cycle. For example, when substituted cysteines in the N-terminal half of the protein close to the first re-entrant domain were labelled with a fluorophore, the fluorescence intensity decreased with hyperpolarizing membrane potentials. This suggested a movement of the fluorophore into a more polar environment occurred, whereas the opposite behaviour was observed after labelling sites in the C-terminal half, close to the second re-entrant segment [42]. These findings hint at a functional coupling between these domains; however, a direct association was not demonstrated.

To obtain more functional evidence of domain interaction, we extended our previous study over a wide voltage range to quantitate the leak and cotransport modes so that conformational states are better defined and substrate interactions more easily identified. In addition to conventional steady-state and presteady-state analysis, we have applied voltage clamp fluorometry assays to examine substrate- and voltage-dependent local interactions with reporter fluorophores and we have investigated the effect of inducing disulfide bridge formation using *Xenopus laevis* oocytes expressing functional flounder NaPi-IIb transporters. Sites were chosen for Cys substitution for fluorophore labelling or to test for disulfide bridge formation that corresponded to the equivalent sites described in our previous studies on the rat NaPi-IIa and flounder NaPi-IIb isoforms. Two sites (Ser155, Ala175) were located in the first (outward facing) re-entrant domain in the N-terminal half of the protein and one site (Ser448) was located in the C-terminal half of the protein at the end of the second (inward facing) re-entrant domain (Fig. 1a).

Our data provide new evidence that supports the involvement of these regions in voltage-dependent, substrate interactions. Moreover, we show that sites associated with the domains come in close contact during substrate translocation, which suggests that SLC34 proteins may share an inverted *trans* re-entrant architecture analogous to that found, for example, in the bacterial Glt_{Ph}, (e.g. [22, 46]).

Methods

Solutions and reagents

Standard extracellular solution (100Na) contained (in millimolars): 100 NaCl, 2 KCl, 1.0 $MgCl_2$, 1.8 $CaCl_2$, 10 HEPES and pH 7.4 adjusted with TRIS base. In Na^+ substitution experiments NaCl was equimolarly replaced with choline Cl (0Na) and solutions with intermediate $[Na^+]$ were obtained by mixing 100Na with 0Na in appropriate portions to maintain a constant molarity. P_i was added from a 1 M K_2HPO_4/KH_2PO_4 stock premixed to give pH 7.4. Phosphonoformic acid (PFA) was added from a 100-mM stock to give the final concentration of 1 mM. Modified Barth's solution for storing oocytes contained (in millimolars): 88 NaCl, 1 KCl, 0.41 $CaCl_2$, 0.82 $MgSO_4$, 2.5 $NaHCO_3$, 2 $Ca(NO_3)_2$, 7.5 HEPES and pH 7.5 adjusted with Tris and supplemented with 5 mg/l doxycyclin and 5 mg/l gentamicin. All standard reagents were obtained from either Sigma-Aldrich or Fluka (Buchs, Switzerland). [2-(trimethylammonium) ethylmethanethiosulfonate bromide (MTSET) was obtained from Toronto Research Chemicals or Biotium (USA); 2-((5(6)-tetramethylrhodamine)carboxylamino) ethyl methanethiosulfonate (MTS-TAMRA) was obtained from Biotium (USA).

Site-directed mutagenesis and cRNA preparation

cDNA encoding wild-type (WT) flounder (fl) NaPi-IIb (GenBank/EMBL/DDBJ accession no AAB16821) was subcloned into a vector containing the 5′ and 3′ UTRs from *Xenopus* β-globin to improve expression in oocytes [41]. Novel cysteines were introduced using the Quickchange site-directed mutagenesis kit (Stratagene Inc.). The sequence was verified by sequencing (Microsynth, Switzerland), and the plasmid was linearised with *Xba*I. The cRNA was synthesised in presence of Cap analogue using the T3 Message Machine kit (Ambion).

Expression in *X. laevis* oocytes

Female *X. laevis* frogs were purchased from *Xenopus* Express (France) or African *Xenopus* Facility (R. South Africa). Portions of ovaries were surgically removed from frogs anaesthetised in MS222 (tricaine methansulphonate) and cut in small pieces. Oocytes were treated for 45 min with collagenase (crude type 1A) 1 mg/ml in 100Na solution (without Ca^{2+}) in presence of 0.1 mg/ml trypsin inhibitor type III-O. Healthy stage V–VI oocytes were selected, maintained in modified Barth's solution at 16°C and injected with 10 ng of cRNA. Experiments were performed 4–7 days after injection. All animal procedures were conducted in accordance with the Swiss Cantonal and Federal legislation relating to animal experimentation.

Two-electrode voltage clamp

The standard two-electrode voltage clamp technique was used as previously described [12, 13]. For recordings at constant holding potential, currents were acquired at >20 samples/s and filtered at 10 Hz. Faster sampling rates (up to 20 k samples/s) were used for voltage step recordings with

filtering adjusted accordingly. Steady-state P_i activation was determined by varying the P_i concentration in presence of 100Na and subtracting the respective currents in 100Na from those in 100Na+P_i. Steady-state Na^+ activation was similarly determined by subtracting the respective responses in XNa from those in XNa+P_i (1 mM), where X is the test Na^+ concentration (in millimolars). Steady-state P_i-induced currents (I_{Pi}) were fit with a form of the modified Hill Equation:

$$I_{Pi} = I_{Pi}^{max}\left([S]^H / \left([S]^H + (K_{0.5}^S)^H\right)\right) + K \quad (1)$$

where [S] is the concentration of variable substrate (Na^+ or P_i), I_{Pi}^{max} is the maximal electrogenic activity, $K_{0.5}^S$ is the apparent affinity constant for substrate S, H is the Hill coefficient and k is a constant that takes into account of uncoupled leak effects [9]. For P_i activation, the Michaelian form of Eq. 1 was used with H=1. Leak current (I_{leak}) in the absence of P_i was determined from the response to 1 mM PFA (in 100Na) such that $I_{leak}=-I_{PFA}$.

Presteady-state relaxations were recorded using voltage steps from V_h=−60 mV to voltages in the range of −180 to +80 mV. Relaxations were quantified by fitting with a two-component exponential function. Typically, the faster time constant was in the range 0.6–0.8 ms and showed no significant voltage dependence, whereas the slower time constant was typically fourfold slower and was voltage dependent. The faster component, which arises from the endogenous linear capacitive charging of the oocyte membrane, was subtracted from the total relaxation to obtain the NaPi-II-dependent component. This was numerically integrated to obtain the charge moved (Q) for a step from the holding potential to the test potential. The Q–V data were fitted with a Boltzmann function of the form given by Eq. 2:

$$Q = Q_{hyp} + Q_{max}/(1 + \exp(ze(V_{0.5} - V)/kT)) \quad (2)$$

where $V_{0.5}$ is the voltage at which the charge is distributed equally between two hypothetical states, z is the apparent valence of an equivalent charge that moves through the whole of the membrane field, Q_{max} is the total charge available to move, Q_{hyp} is the charge of the hyperpolarizing limit and is a function of V_h and e, k and T have their usual meanings.

^{32}P uptake

Oocytes expressing flNaPi-IIb Cys mutants (six to ten oocytes/group) were first allowed to equilibrate in 100Na solution without tracer. After aspiration of this solution, oocytes were incubated in 100Na solution containing 1 mM cold P_i and ^{32}P (specific activity 10 mCi/mmol P_i). Uptake proceeded for 10 min and then oocytes were washed three to four times with ice-cold 0Na solution containing 2 mM P_i, and lysed individually in 10% SDS for 1 h before addition of scintillation cocktail. The amount of radioactivity in each oocyte was measured by scintillation counting.

Simultaneous voltage clamp and fluorometry

The apparatus for simultaneous VCF has been described in detail elsewhere [42, 43]. Cysteine mutants were labelled in 100Na in the presence of MTS-TAMRA (0.4 mM) at room temperature. Voltage-dependent changes in fluorescence (ΔF) were determined using a voltage step protocol. The membrane voltage was stepped from V_h=−60 mV to test potentials ranging between −200 mV and +200 mV in 40 mV increments for a duration of 100–200 ms, and averaged over 20–64 sweeps. ΔF was measured in 100Na, 0Na and 100Na +1P_i (100 mM Na^+ + 1 mM P_i); each test substrate concentration application was bracketed with a control solution application (100Na) to allow for correction of a loss of fluorescence. After application of the superfusate the oocyte was allowed to stabilise in the recording chamber for ~2 min and then fluorescence was recorded. Recordings were baseline corrected relative to the value at V_h=−60 mV. After correction for photobleaching, the data from single oocytes were normalised to the predicted maximum change in fluorescence (ΔF_{max}) recorded in 100Na and then pooled. ΔF_{max} was obtained from the ΔF–V data fitted with the Boltzmann equation (Eq. 2, where Q was substituted with ΔF).

Thiol modification by MTSET

MTSET was added to 100Na solution from a 1 M stock (in water, stored at −20°C) to give a final concentration of 1 mM. MTSET was applied to the recording chamber with gravity feed via a 0.5-mm-diameter cannula positioned near the cell. Incubation time was 3 min and was followed by a 1-min washout period. During superfusion with MTSET, oocytes were voltage clamped at V_h=−50 mV. After washout, the P_i-induced current was measured.

Inhibition by copper(II)(1,10-phenanthroline)$_3$

The Cu(II) (1,10-phenanthroline)$_3$ ($CuPh_3$) stock solution was prepared for each experiment by mixing 40 μl of 1.25 M 1,10-phenanthroline (dissolved in water/ethanol 1:1) and 60 μl of 250 mM $CuSO_4$. For ^{32}P uptake, groups of 12 oocytes from two different batches were pre-incubated in 0.2 mM $CuPh_3$ for 5 min and then washed in 100Na. Half of these were further incubated in dithiothreitol (DTT; 10 mM) for 10 min and washed again in 100Na (5 min). After washing, 100Na was replaced with the uptake solution. Uptake was performed as described above.

For TEVC experiments, P_i-induced current was first measured in control condition (100Na). P_i-induced current was measured again after incubation of the oocytes in $CuPh_3$ 0.2 mM for 5 min (in 100Na or 0Na). For DTT treatment, oocytes were treated for 10 min with freshly prepared 12 mM DTT (in 100Na) after incubation with $CuPh_3$ and then washed and tested. Oocytes were removed from the recording chamber for incubation to avoid irreversible deterioration of electrodes by DTT.

Software and data analysis

Simulations of a ten-state model describing electrogenic cotransport were performed using Berkeley Madonna V8.0.2a8 software (www.berkeleymadonna.com). All curve fitting was performed using GraphPad Prism version 3.02/4.02 for Windows (GraphPad Software, San Diego California USA, www.graphpad.com). Data points are shown as mean ± SEM. Error bars are not displayed if smaller than symbol.

Results

Cysteine substitutions and thiol modification alter transport kinetics

Steady-state behaviour After expression in *X. laevis* oocytes, the single (S155C, A175C and S448C) and double (S155C-S448C, A175C-S448C and A175S-S448C) mutants, gave robust P_i-induced currents in the presence of external Na^+ (100Na solution) in the range −50 to −300 nA, when voltage clamped to V_h=−50 mV. To determine if and how the Cys substitution affected the cotransport activity, we estimated the apparent affinity constants for P_i activation (with 100 mM Na^+ (100Na)) ($K_{0.5}^{Pi}$) and Na^+-activation ($K_{0.5}^{Na}$ with 1 mM P_i) by measuring the P_i-induced current (I_{Pi}) under different superfusing conditions as previously described (e.g. [13, 40]). The data in both cases were reliably fitted using Eq. 1. The Cys substitution did not significantly affect $K_{0.5}^{Pi}$ for any of the constructs, whereas we observed a significant increase in $K_{0.5}^{Na}$ for A175C at 0 mV and −100 mV (Table 1).

To investigate the effect of Cys substitution and subsequent modification of the introduced cysteines on voltage-dependent kinetics, we first determined the steady-state voltage dependence of the leak current (I_{leak}) and the cotransport current (I_{cot}) before and after exposure to the membrane impermeable MTSET (1 mM, 3 min or until the change in I_{Pi} reached a steady-state). I_{leak} was estimated by measuring the change in holding current induced by 1 mM of the Na^+-P_i cotransport inhibitor, phosphonoformic acid (PFA) (I_{leak}=−I_{PFA}); I_{cot} was obtained from (I_{cot}=I_{Pi}+I_{leak}) as previously described [3, 10]. The determination of the cotransport activity by this procedure assumed that 1 mM P_i or 1 mM PFA were sufficient to suppress the leak mode completely (e.g. [3, 9]). Figure 2 shows *I–V* data normalised to I_{Pi} at −100 mV before MTSET application to facilitate comparison of the voltage dependences.

To quantify changes in voltage dependence on cotransport activity caused by mutagenesis itself, we compared the normalised I_{cot} at V=0 relative to V=−100 mV. The ratio was used as a steady-state voltage dependence index (indicated in each panel of Fig. 2). For the single mutants (Fig. 2a), these data show that although Cys substitution at 175 was tolerated, the voltage dependence was significantly altered, whereby $I_{cot}^{0}/I_{cot}^{-100}$ was reduced from 0.41 (WT) to 0.10 (A175C). This behaviour was also observed in the voltage dependence of I_{leak} for this mutant. In contrast, Cys substitution at sites 155 or 448 had a small and opposite effect on the voltage dependence of I_{cot} as indicated by the increase in $I_{cot}^{0}/I_{cot}^{-100}$ compared to the WT: both S155C and S448C showed more saturation of I_{cot} at hyperpolarizing potentials, which was reflected in their larger $I_{cot}^{0}/I_{cot}^{-100}$ (Fig. 2a).

The *I–V* data of S155C-S448C and A175C-S448C (Fig. 2b) showed mixed behaviour, depending on the site of substitution in the first re-entrant domain. For S155C-S448C, $I_{cot}^{0}/I_{cot}^{-100}$ lay close to the values for the corresponding single mutants, whereas for A175C-S448C, $I_{cot}^{0}/I_{cot}^{-100}$ was significantly larger than that of A175C.

The altered voltage dependences of A175C and A175C-S448C compared to the WT prompted us to investigate in more detail the role site 175 might play in determining this kinetic parameter. We replaced Ala175 with Ser, Leu, Asp and Arg in the S448C background. Only one double mutant (A175S-S448C) gave measurable I_{Pi}. For A175S-S448C, analysis of substrate activation data in the cotransport mode gave apparent affinity constants $K_{0.5}^{Pi}$ and $K_{0.5}^{Na}$ that were indistinguishable from the WT (Table 1). This result indicated that the Ser substitution was well tolerated, and its $I_{cot}^{0}/I_{cot}^{-100}$ approached the WT value.

Of the three single mutants, only S448C showed a significant change in behaviour after MTSET incubation, as previously reported [43] and is consistent with that of the equivalent mutation (S460C) in the rat NaPi-IIa isoform [23]. After Cys modification, I_{Pi} was fully suppressed and was outwardly directed, whereas, I_{leak} remained unchanged Fig. 2a. I_{cot} was therefore close to zero, consistent with only the leak mode being active after Cys modification; i.e. with suppressed cotransport activity, the action of P_i and PFA are indistinguishable [20]. For S155C, as previously reported [42], we observed no significant change in I_{Pi}, even though this site is considered accessible to MTS reagents [33, 42]. A175C showed only a small decrease in I_{Pi} and no change in I_{leak} (Fig. 2a).

The double mutants containing Cys-448 showed qualitatively similar behaviour after MTSET incubation: like

Table 1 Steady-state apparent affinity constants at −100 and 0 mV

	−100 mV		0 mV	
	$K_{0.5}^{Pi\ a}$	$K_{0.5}^{Na\ b}$	$K_{0.5}^{Pi\ a}$	$K_{0.5}^{Na\ b}$
WT	0.048±0.015	35.3±4.5	0.043±0.011	58.0±6.3
A175C	0.050±0.005	57.3±4.8[e]	0.048±0.001	91.7±3.2[e]
A175C-S448C	0.055±0.005	42.9±4.2	0.049±0.001	60.6±8.7
A175S-S448C	0.066±0.012	38.9±8.6	0.057±0.030	48.4±3.5
S155C[c]	0.068±0.012	n.d.	0.052±0.009	n.d.
S155C-S448C	0.040±0.002	37.1±3.8	0.037±0.004	48.3±3.5
S448C[d]	0.047±0.009	25.9±2.5	0.039±0.008	53.8±3.9

Apparent affinity constants for P_i ($K_{0.5}^{Pi}$) or Na^+ ($K_{0.5}^{Na}$) determined from fits using Eq. 1 to P_i or Na dose dependence of I_{Pi}. Values (in mM) are given as mean ± SEM as reported by fitting algorithm from pooled, normalised data ($n \geq 5$)

n.d. not determined

[a] Determined in 100Na

[b] Determined with 1 mM P_i

[c] Values from [42]

[d] Values from [43]

[e] Statistically significant compared to WT (Student's *t* test, $p \leq 0.01$)

S448C their cotransport activity was suppressed (Fig. 2b). In accord with our earlier study using the rat NaPi-IIa isoform [20], A175C-S448C showed an increased I_{leak} with an apparent outward I_{Pi} that had approximately the same magnitude as I_{leak} after MTSET exposure, whereas both S155C-S448C and A175S-S448C showed no resolvable change I_{leak}.

Presteady-state behaviour To identify the partial reactions in the transport cycle responsible for the shifts in steady-state voltage dependence, we investigated the presteady-state kinetics. Voltage dependence of NaPi-II proteins is proposed to arise from partial reactions in the transport cycle that involve charge translocation, specifically from the binding/release of substrates (Na^+ ions) and intrinsic voltage-dependent conformational changes of the protein (e.g. [12, 13]). These partial reactions can be investigated by applying voltage steps under different superfusate conditions and analysing the resulting presteady-state relaxations, after elimination of the linear capacitive charging transient.

For a representative oocyte expressing the WT and superfused in 100Na (Fig. 3a), the transient currents in response to equal but opposite voltage steps, showed a characteristic asymmetry that depended on the direction of the voltage step from the holding potential (V_h=−60 mV). More charge was displaced for a depolarizing step than for the same magnitude hyperpolarizing step. The single mutants S448C and S155C as well as S155C-S448C showed similar behaviour to the WT (data not shown). In contrast, A175C and A175C-S448C (Fig. 3a) showed relaxations with the opposite behaviour, whereby more charge was displaced for the hyperpolarizing step compared with the depolarizing step. This behaviour matched the shift in steady-state voltage dependence of I_{Pi} towards hyperpolarizing potentials (Fig. 2). A175S-S448C gave presteady-state relaxations similar to the WT (not shown). The main relaxation time constants varied in the range from 2.5 to 7.5 ms and their voltage dependence in 100Na depended on the site of cysteine mutagenesis.

To determine if the altered voltage dependence arose from changes to the kinetics of the empty carrier, Na^+ ion interaction or both, we examined the Na^+-dependence of presteady-state currents by exposing the oocytes to solutions with different Na^+ concentrations. For each condition, the charge (Q_{ON}) displaced from −60 mV to each test potential (V) was separated from the linear oocyte capacitive charge movement (see Materials and methods) and plotted as function of V. To facilitate comparison, we normalised the Q–V data to the depolarizing limit estimated from the Boltzmann fit (see below). For the WT (Fig. 3b), Q_{ON} tended to saturate at positive and negative potentials for all [Na^+] as we have previously shown [13, 43] and there was a characteristic hyperpolarizing shift in the charge distribution as Na^+ was progressively replaced by choline. For A175C and A175C-S448C (Fig. 3b), saturation at hyperpolarizing potentials was less apparent except at low [Na^+]. We were unable to step to potentials more negative than −180 mV because the transient currents became contaminated by activating endogenous Cl^- currents or

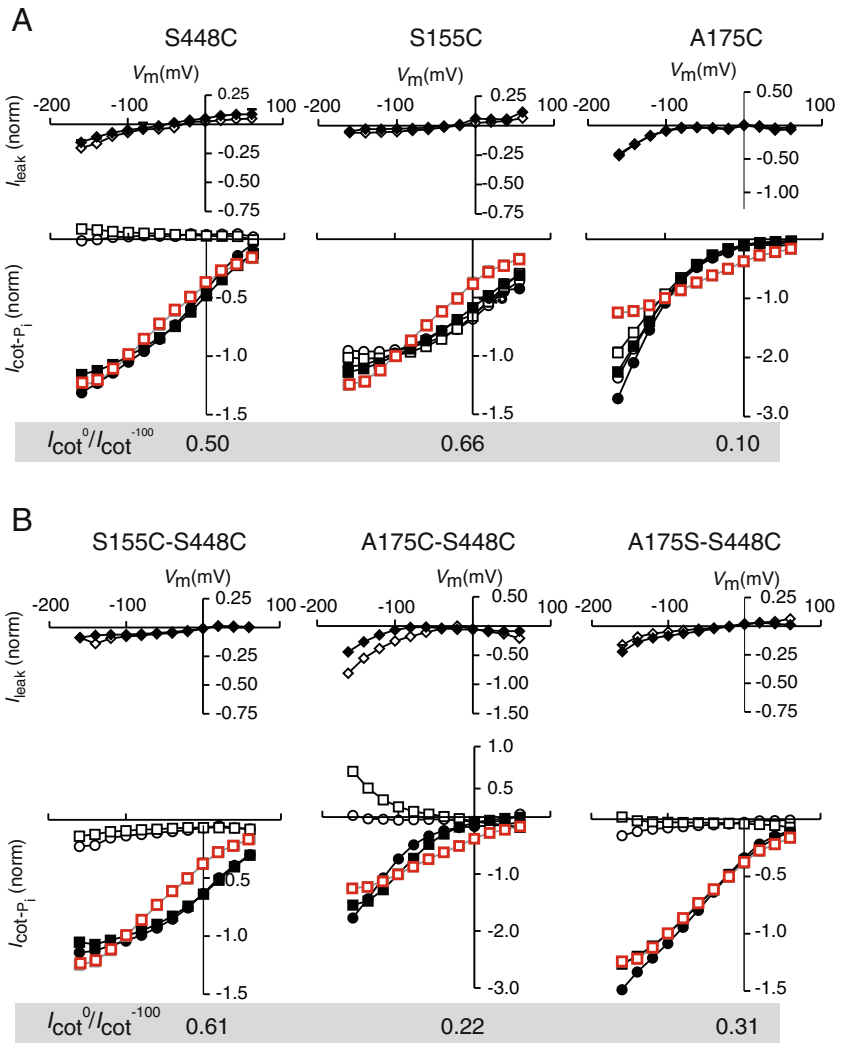

Fig. 2 Cysteine substitution alters NaPi-IIb voltage dependence. **a** Normalised current–voltage (*I–V*) data for single mutants: S448C (*left*), S155C (*centre*) and A175C (*right*). For each construct, the *upper panel* shows the voltage dependence of leak (*diamonds*) given by I_{PFA}. The *lower panel* shows the cotransport-related currents: P_i-induced current (I_{Pi}) (*squares*) and predicted cotransport mode (I_{cot}= I_{Pi}−I_{PFA}) (*circles*). Data sets are shown before (*filled symbols*) and after MTSET incubation (*open symbols*) for I_{cot}, I_{PFA} only. To aid comparison and to show the effect of mutagenesis and Cys modification on the voltage dependence, normalised I_{Pi} data for the WT (before MTSET exposure) are superimposed on each mutant data set (*open red squares*). **b** Current–voltage (*I–V*) curves for double mutants S155C-S448C (*left*), A175C-S448C (*centre*) and A175S-S448C (*right*) showing the leak and transport mode related currents before and after exposure to MTSET. All symbols and nomenclature as in (**a**). Each data point represents the mean of ≥5 oocytes, and data were normalised to I_{Pi} at −100 mV before MTSET incubation. Data points joined for visualisation. The steady-state voltage dependence index (I^0_{cot}/I^{-100}_{cot}) (see text) is indicated for each construct (WT= 0.41). Note that different ordinates are used for A175C and A175C-S448C to account for the larger relative currents at hyperpolarizing potentials compared with the other mutants

the oocyte became irreversibly leaky, thereby making the presteady-state analysis more error prone.

To further characterise the presteady-state data, we fitted them with a form of the Boltzmann equation (Eq. 2, continuous lines (Fig. 3b)) to obtain three parameters: Q_{max}, the maximum charge displaced; $V_{0.5}$, the midpoint voltage and z, the apparent valence (Fig. 3c). The Q_{max} values were normalised to the value obtained at 100 mM Na^+ for each construct to aid comparison of the Na^+-dependence. For the WT, the normalised Q_{max} at 100 mM Na^+ decreased by 20% at 25 mM and then more rapidly to approximately 50% of the maximum in 0Na; $V_{0.5}$ showed the characteristic hyperpolarizing shift that we have previously reported for NaPi-IIb [43] and z reported by the fit lay in the range 0.4–0.6 for all superfusion conditions. For A175C and A175C-S448C the derivation of the Boltzmann parameters was less certain due to the lack of saturation of the charge movement at hyperpolarizing potentials. In particular, for A175C, we constrained z to 0.4 to reduce fit uncertainties. Under these conditions, the dependence of the normalised Q_{max} and $V_{0.5}$ on [Na^+] contrasted significantly with that of the WT for both mutants: Q_{max} increased almost linearly with [Na^+]

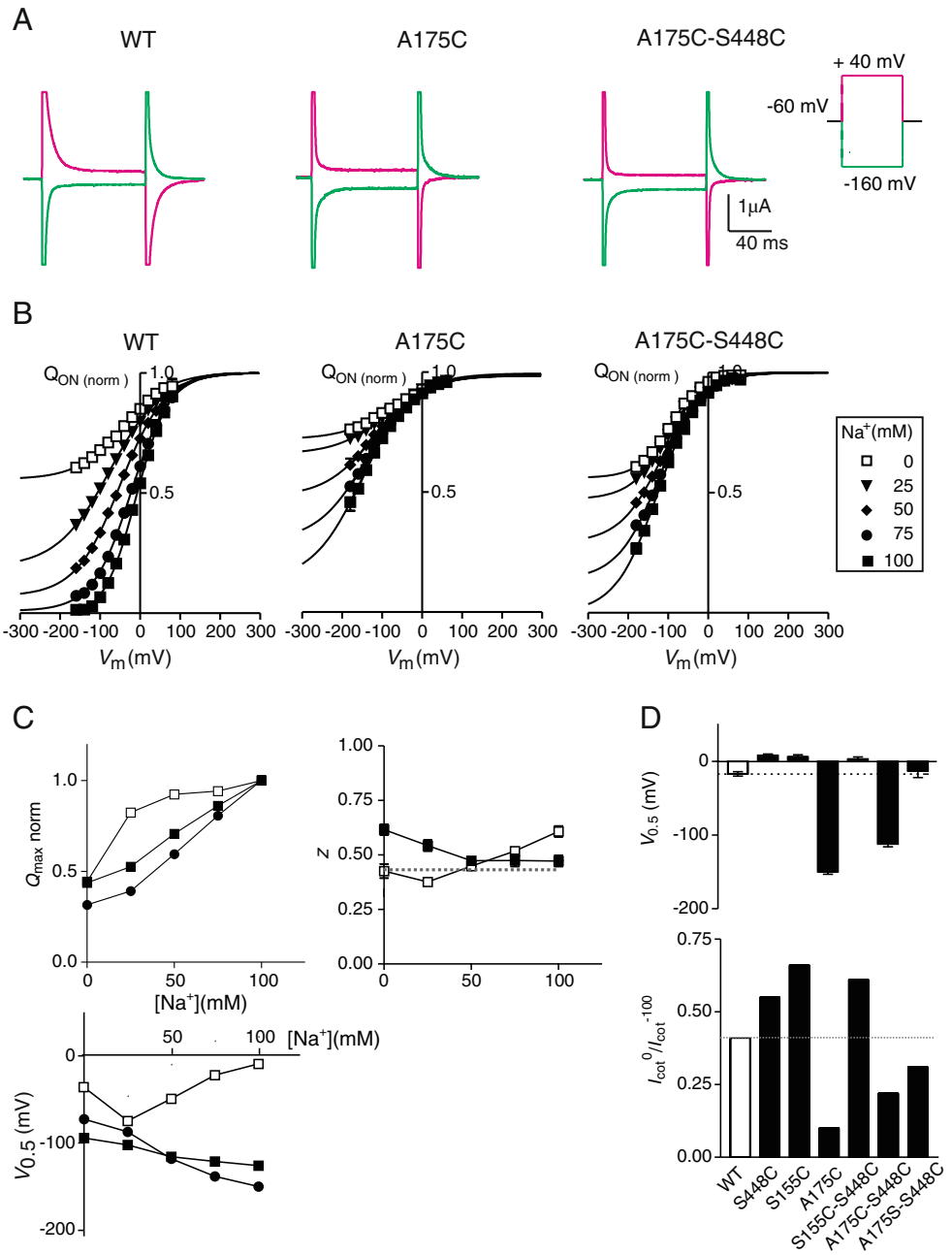

Fig. 3 Presteady-state charge movements indicate that Cys-175 imposes a dominant effect on voltage dependence of Na^+ interaction. **a** Representative current recordings from WT (*left*), A175C (*centre*) and A175C-S448C (*right*) for superfusion in 100 mM Na^+ in response to symmetrical 100 mV depolarizing (*red*) and hyperpolarizing (*green*) steps from the holding potential (−60 mV). **b** Charge (Q_{ON}) for voltage steps from −60 mV to test potential (V) determined from curve fits to presteady-state relaxations, plotted as function of V for different external [Na^+]: WT (*left*), A175C (*centre*) and A175C-S448C (*right*). Continuous lines are fits with Eq. 2. To better visualise the effect of [Na^+] on the midpoint voltage ($V_{0.5}$), the data were offset so that each data set and curve are superimposed at the depolarizing limit predicted from the fit to the 100Na data and normalised. **c** Na^+ dependence of Boltzmann parameters (Q_{max}, z, $V_{0.5}$) predicted from fits to Q–V data plotted as a function of [Na^+]. Each panel shows data for WT (*open squares*), A175C (*filled circles*) and A175C-S448C (*filled squares*). Data points are shown as mean ± SEM (n >4) and joined for visualisation. To emphasise the differences in Na^+ dependence, the Q_{max} values were normalised to the estimate at [Na^+] = 100 mM for each construct. **d** Comparison of steady-state voltage dependence ($I_{cot}^{0}/I_{cot}^{-100}$) and $V_{0.5}$ with 100Na superfusion, for each construct. *Dotted lines* indicate WT mean values

and, unexpectedly, $V_{0.5}$ decreased with increasing [Na^+] (Fig. 3c). In 0 mM Na^+, $V_{0.5}$ was shifted for both A175C and A175C-S448C to more hyperpolarizing potentials, which indicated that the substitution at site 175 had changed the steady-state empty carrier occupancy. At 100 mM Na^+, the shift of $V_{0.5}$ relative to the WT for each mutant correlated with the direction of shift of $I_{cot}{}^0/I_{cot}{}^{-100}$ (Fig. 3d). This result underscored the importance of the presteady-state charge movement kinetics in determining the voltage dependence of the cotransport mode. Presteady-state relaxations were also resolved after Cys modification by MTSET. Neither S155C nor A175C showed significant deviation from the behaviour before MTSET application (data not shown). In contrast, all constructs containing Cys448 showed a significant decrease in the estimated total amount of mobile charge (Q_{max}) for superfusion in 0Na and 100Na and shifts in $V_{0.5}$ that depended on the site mutated in the first re-entrant domain (Table 2).

$CuPh_3$ promotes disulfide bridge formation between pairs of cysteines

Next, we investigated the functional behaviour of the double Cys mutants after inducing disulfide bond formation between the introduced cysteines. This can be catalysed using O_2/Cu (II)(1,10-phenanthroline)$_3$ ($CuPh_3$), whereby the dissolved dioxygen acts as an oxidant and $CuPh_3$ as a redox catalyst [5]. Moreover, the bond formation should be reversible by incubation in a reducing medium, e.g. dithiothrietol. We reasoned that if the two re-entrant domains associate to form the pathway for the translocation of the substrate, formation of a disulphide bond should interfere with the normal conformational changes associated with translocation of the substrate and therefore result in a change in I_{Pi}.

We first analysed the effect of incubation with $CuPh_3$ on single and double mutants using ^{32}P uptake (Fig. 4a). Neither $CuPh_3$ nor incubation in DTT affected P_i uptake mediated by A175C, S155C and S448C (Fig. 4a) or the WT (data not shown). This finding confirmed that the introduced cysteines did not interact with any of the 11 endogenous cysteines that are present in flNaPi-IIb. Nevertheless, we cannot exclude the possibility that such disulfide bonds were formed but had no effect on transport function. In contrast, for S155C-S448C and A175C-S448C, treatment with $CuPh_3$ caused reductions in ^{32}P uptake of 50% and 40%, respectively. Moreover, this inhibition could be reversed by subsequent incubation of the oocytes with DTT (Fig. 4a, *grey bars*) in support of the hypothesis that the inhibition of the transport was due to disulfide bridge formation between the pairs of introduced cysteines.

From this and other studies there is strong evidence obtained from presteady-state and voltage clamp fluorometric assays that NaPi-II proteins undergo conformation changes dependent on the substrate availability that involves the re-entrant domains. We therefore investigated if the presence or absence of substrate could affect the likelihood of disulfide bridge formation by changing the state of the protein during $CuPh_3$ incubation. Individual oocytes were assayed under voltage clamp (V_h=−50 mV) before and after exposure to $CuPh_3$ and DTT in 0Na or 100Na. We did not perform these assays with preincubation in 100Na+1P_i due to a loss of transport activity, which results from internalisation of transporters following repeated and extended application of P_i (e.g. [34]).

Consistent with uptake data, the single mutants showed no significant change in I_{Pi} after preincubation in $CuPh_3$ with either 0Na or 100Na (Fig. 4b). In contrast, when S155C-S448C or A175C-S448C was incubated in 100Na+ $CuPh_3$, we observed a decrease of I_{Pi} of ~50% and 40%,

Table 2 Comparison of Boltzmann parameters for presteady-state and fluorescence

Construct	$Q_{max}{}^{+MTSET}/Q_{max}{}^{-MTSET}$		$V_{0.5}$ (mV)[b]		$V_{0.5}{}^F$ (mV)[b]	z^b		$z^{F\ b}$
	0Na	100Na	−MTSET	+MTSET	+MTS-TAMRA	−MTSET	+MTSET	+MTS-TAMRA
WT	1.00	1.00	−17±3	−15±2	–	0.68±0.05	0.69±0.05	–
S448C	0.45	0.56	8±2	−6±9	−197±17	0.60±0.03	0.42±0.06	0.30±0.02
S155C	0.91	1.00	6±3	−8±2	−38±1	0.61±0.03	0.56±0.04	0.49±0.01
S155C-S448C	0.40	0.45	3±3	−28±4	−230±5	0.67±0.05	0.59±0.05	0.20±0.01
A175C	0.91	0.91	−198±16	−178±10	n.a	0.4[a]	0.4[a]	n.a
A175C-S448C	0.48	0.59	−112±4	−52±5	−42±5	0.64±0.02	0.56±0.04	0.26±0.02
A175S-S448C	0.42	0.43	−13±9	4±9	−81±4	0.67±0.07	0.57±0.12	0.4±0.02

n.a. not applicable

[a] z constrained to 0.4 for fit

[b] Values determined in100Na

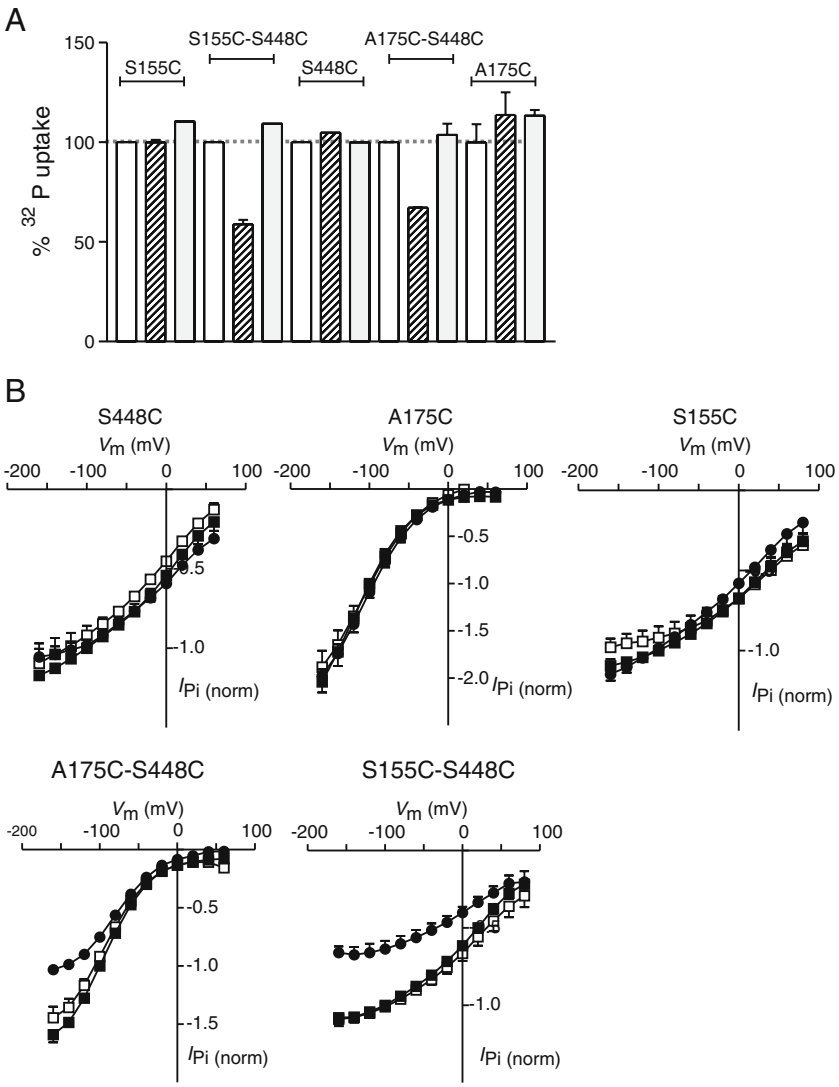

Fig. 4 Effect of $CuPh_3$ on cotransport activity for single and double mutants. **a** ^{32}P uptake was measured on groups of oocytes ($n>5$) in control condition (*empty bars*), after incubation in $CuPh_3$ (*cross hatched bars*) and after incubation in $CuPh_3$ followed by incubation in DTT (*grey bars*). Data are shown as mean ± SEM. **b** *I–V* data showing I_{Pi} for mutants indicated was measured in control condition (*filled squares*), after incubation in $CuPh_3$ in 100 mM Na^+ (*filled circles*) or after incubation in 0 mM Na^+ (*empty squares*). Data were normalised to I_{Pi} at −100 mV before incubation. Points are joined for visualisation

respectively. Longer incubation periods did not result in a further decrease in current, whereas subsequent application of MTSET suppressed I_{Pi} (data not shown). Moreover, for incubation with 0Na+$CuPh_3$, no significant change in I_{Pi} was measured for S155C-S448C, whereas there was a small decrease for A175C-S448C at hyperpolarizing potentials. To confirm that the loss of function observed for the double mutants occurred as a result of cross-linking within each NaPi-II monomer, and not between adjacent monomers, we co-expressed the A175C or S155C together with S448C and incubated the oocytes in $CuPh_3$ as above. No change in function was observed. Despite the obvious loss of transport function after $CuPh_3$ treatment, we detected no significant change in the presteady-state charge movement (Q_{max}, $V_{0.5}$ and z; data not shown) for the double mutants. This result indicated that the disulfide bridge formation had neither altered the voltage dependence of the empty carrier nor Na^+ interactions.

Substrate- and voltage-dependent changes in fluorescence intensities

To further investigate functional interactions between the two re-entrant domains, we applied voltage clamp fluorometry that we have previously demonstrated to be useful in observing local conformational changes of NaPi-II proteins [14, 42, 43]. The rationale for these experiments was that if the two re-entrant domains interact, structural changes induced by mutagenesis in one domain may directly alter the microenvironment of the reporter fluorophore in the other domain. Oocytes expressing single or double mutants were incubated in MTS-TAMRA (0.4 mM, 5 min) and we measured changes in fluorescent intensity (ΔF) in response to step changes in the membrane potential. As substrates are assumed to place the protein in different conformational states that may alter the relative position of the re-entrant domains,

we compared the fluorescence with superfusion in 0Na, 100Na and 100Na+1P_i.

Figure 5 compares the fluorescence recorded from representative oocytes expressing the respective mutant transporters in response to voltage steps from V_h=−60 mV to three test potentials: −160, 0 and +80 mV. The data show that ΔF–V varied, depending on the construct and the superfusion conditions. For all constructs, depolarizing voltage steps induced an increase in fluorescence intensity relative to that at V_h. With the notable exception of A175C, all constructs gave robust ΔF in 100Na of comparable magnitude, whereas the responses of the same oocyte in 0Na and 100Na+1P_i were different. For example, oocytes expressing S448C showed no detectable ΔF in 0Na, whereas ΔF was resolved in 100Na and 100Na+1P_i. In contrast, oocytes expressing A175C-S448C showed a robust ΔF in 0Na and 100Na but no detectable ΔF in 100Na+1P_i. It should be noted that the functional consequences of labelling with the fluorophore (e.g. suppression of I_{Pi} in the case of S448C) were the same as found for incubation in MTSET (data not shown). Moreover, we also observed that no ΔF could be resolved if oocytes were pre-incubated in MTSET before labelling with the fluorophore, which confirmed that the target Cys

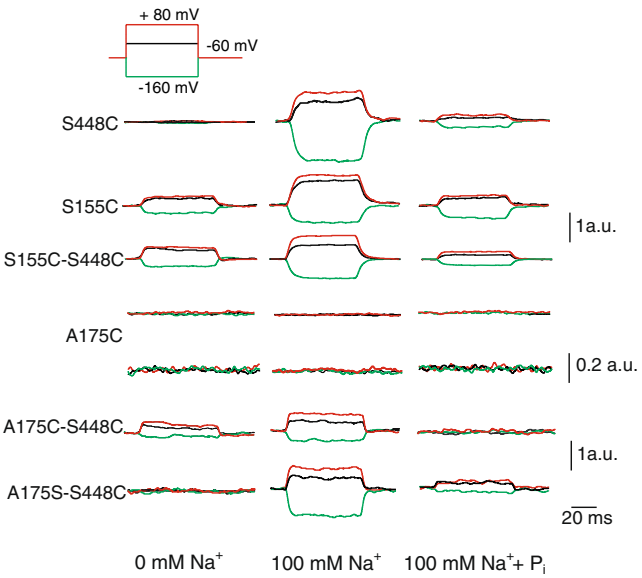

Fig. 5 Voltage-dependent changes in fluorescence intensity (ΔF) depend on superfusate. Representative data recorded for voltage steps from −60 to −160 mV (*green*), 0 (*black*) and +80 mV (*red*) for the constructs indicated. Each data set represents recordings from the same oocyte expressing the respective mutant under different superfusion conditions. Note that for A175C, the same data with two scale factors are shown to indicate that no detectable ΔF was observed for this mutant. *au* arbitrary unit of fluorescence intensity. The fractional change in fluorescence $\Delta F/F$ for all constructs was typically 0.01 for one a.u, and depended on the expression level of the individual oocytes

was most likely the same as for MTSET. After correcting for the loss of fluorescence due to bleaching or washout (Materials and methods), the magnitude of ΔF observed for each superfusate was found to be independent of the order of application of the particular superfusate, thereby confirming that we were observing a memoryless process. The absence of detectable ΔF for oocytes expressing A175C suggested either that the site was also inaccessible to MTS-TAMRA, consistent with the insensitivity of I_{Pi} to MTSET exposure (Fig. 2b) or if labelled, that the microenvironment of the fluorophore at this site did not change sufficiently to yield detectable fluorescence intensity changes.

We obtained further insight into the voltage and substrate dependence of fluorescence by recording ΔF for voltage steps over a wide voltage range and used extensive signal averaging to improve the signal-to-noise ratio (see Materials and methods). To aid comparison of the voltage dependence of fluorescence intensity, ΔF–V data (Fig. 6) pooled from several batches of oocytes were normalised to ΔF_{max} predicted from fits using Eq. 2. Fit parameters are summarised in Table 2.

S155C, S448C and S155C-S448C (Fig. 6a) In 0Na, S155C and S155C-S448C showed similar ΔF–V with no saturation at the hyperpolarizing extreme. This behaviour suggested that the fluorophores reported ΔF consistent with both Cys155 and Cys448 being successfully labelled in the double mutant, in contrast to the lack of detectable ΔF for S448C under the same conditions. For superfusion in 100Na, S155C-S448C showed similar behaviour to S448C with no saturation at the hyperpolarizing extreme. This contrasted with the behaviour of S155C, which yielded a sigmoidal ΔF–V relationship within the voltage range explored. Finally, with 100Na+1P_i, the ΔF–V relation for S155C-S448C resembled that of S448C; compared to S155C, there was reduced ΔF over the same voltage range and no obvious sigmoidicity in its voltage dependence.

A175C-S448C, A175S-S448C and S448C (Fig. 6b) ΔF recorded from oocytes expressing A175C-S448C showed a substrate and voltage dependence very different from S448C: for 0Na and 100Na, its ΔF–V relation was sigmoidal, and adding Na^+ to the medium caused a ~20 mV depolarizing shift in the midpoint voltage ($V_{0.5}^F$; Table 2). In 100Na+1P_i, we resolved no ΔF over the range of potentials explored. ΔF was also detectable with the double mutant A175S-S448C, which depended on the superfusion conditions. Like S448C, no ΔF was detectable for superfusion in 0Na, whereas superfusion in 100Na gave a sigmoidal ΔF–V relationship similar to A175C-S448C, but with a larger z^F and a hyperpolarizing shift of ~40 mV in $V_{0.5}^F$ (Table 2). In 100Na+1P_i, its ΔF–V relation was similar to that of S448C.

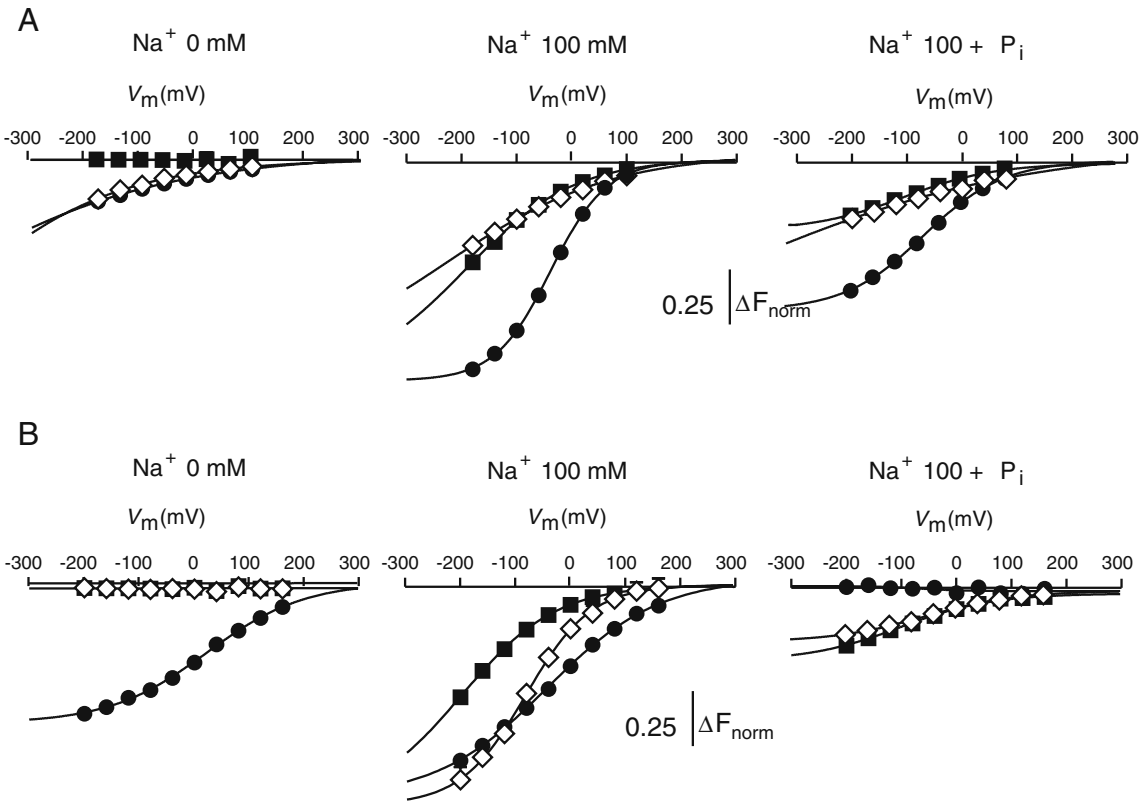

Fig. 6 Substrate- and voltage-dependent changes in fluorescence intensity. **a** Voltage-dependent change in fluorescence intensity (ΔF) for S448C (*filled squares*), S155C (*open circles*) and A155C-S448C (*open diamonds*) compared for three superfusion conditions: 0 mM Na^+ (*left panel*), 100 mM Na^+ (*centre panel*) and 100 mM Na^+ + 1 mM P_i *(right panel*). Data points and fits were adjusted so that they superimposed at the depolarizing limit. For each construct, ΔF data were normalised to ΔF_{max} in100 mM Na^+ predicted from a fit using a single Boltzmann function (Eq. 2). Each data point represents mean ± SEM with $n \geq 3$ cells. *Error bars* were smaller than symbols. **b** Voltage-dependent change in fluorescence intensity (ΔF) for S448C (*filled squares*) compared with A175C-S448C (*filled circles*) and A175S-S448C (*open diamonds*) for three superfusion conditions as in (**a**)

Discussion

The identification of the transport pathway and sites of substrate binding in membrane carrier proteins is of crucial importance to understand cotransport mechanisms at the molecular level. 3-D structures of crystallised bacterial homologs of mammalian Na^+-dependent cotransporters that belong to different gene families reveal a common structural motif: an inverted repeat topology in which the respective elements are structurally associated through an apparent twofold symmetry around an axis through the membrane plane. This common architecture defines a central substrate translocation pathway with the substrate binding sites located approximately halfway through the membrane and accessible from either side of the membrane, consistent with the alternating access model for carrier-mediated transport [1, 11, 22]. Pairs of discontinuous helices play a key structure-functional role in this architecture [36]. These can be either transmembrane spanning, as found in $LeuT_{Aa}$ [45] and *v*SGLT [2] or hairpin (re-entrant) as found in ClC [8] and GlT_{Ph} [46]. The short peptide linkers between the helices are critical for substrate recognition and coordination. The ubiquity of these common architectures among genetically unrelated transporters is underscored by studies comparing hydropathies of the core regions that propose classification based on similarity of structural folds [28, 29].

Given that many transporters share a common functionality—i.e. coupling to the electrochemical gradient of Na^+ to catalyse uphill movement of a specific substrate—it follows that the same architecture may be present in transport proteins whose 3-D structures have yet to be resolved. For the SLC34 family and related bacterial homologs, no crystal structure is currently available and their low homology with proteins of known structure has so far precluded successful homology modelling. Nevertheless, the existence in all members of the SLC34 family of the common repeat region in the N- and C-terminal halves of the proteins (Fig. 1b) offers compelling evidence that these regions may also be involved in the formation of the transport pathway. This conclusion has been the basis of a number of functional studies focussing on these regions

[19, 20, 24]. For example, evidence that the re-entrant domains play a functional role in co-determining the transport mode (leak or cotransport) was found for the rat NaPi-IIa isoform, based on the behaviour of a double Cys mutant (corresponding to A175C-S448C in the present study) [20].

Here we have taken a functional approach to: (1) characterise the role these putative re-entrant domains play in defining the kinetics of the transport cycle and (2) test for interactions between the domains for a representative member of the SLC34 Na^+-coupled P_i transporter family. We have focussed on changes in substrate- and voltage-dependence of the transport function because these are considered strong determinants of implied conformational changes. In the context of structure–function relationships it is helpful to consider the transport properties of electrogenic SLC34 proteins in terms of a ten-state kinetic scheme to which our experimental findings can be referred (Fig. 7). This model depicts the two modes of electrogenic activity, leak and cotransport as a cyclic sequence of partial reactions, some of which (empty carrier and Na^+-interaction partial reactions) are common to both modes [3]. A feature of this model is that the electrogenicity of both the leak and cotransport cycles arises only from mobile charges associated with the empty carrier transition (1↔8), assumed to be intrinsic to the protein, and the first Na^+ interaction (1↔2a, 8↔7a). We assumed that all other partial reactions were electroneutral in this scheme. One aim of structure–function studies is to determine the relationship between structural elements and the partial reactions in such a scheme.

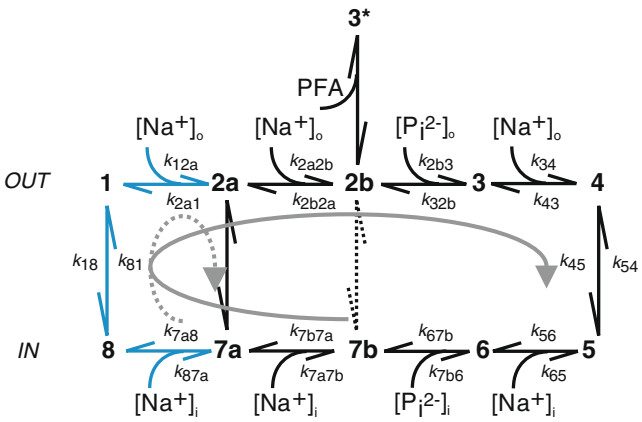

Fig. 7 Ten state kinetic scheme for the electrogenic leak and cotransport modes for SLC34 proteins. Each state is assumed to represent a unique conformation of the protein. Transitions between states are described in terms of forward and backward rate constants that for certain transitions are substrate or voltage dependent (Table 3). This model assumes only the empty carrier (1↔8) and first Na binding partial reactions (1↔2a; 8↔7a) involve charge movement (*blue*). The two transport modes (leak and cotransport) share these transitions. PFA is assumed to place in the protein in a dead-end state

Cysteine mutagenesis: identification of a site in putative re-entrant domain 1 implicated in Na^+ interactions and voltage dependence

Single Cys substitutions affected the voltage dependence of the mutant constructs at all three sites, but to varying degrees. Substitutions at 155 and 448, sites predicted to be exposed to the external medium, had relatively small effects: both shifted the steady-state voltage dependence of I_{Pi} towards depolarizing potentials relative to the WT. For these mutants, any small changes in the voltage dependence of I_{leak} relative to the WT, which we would predict according to our kinetic scheme, were not easily resolved due to the small magnitude of this current. In contrast, Cys substitution at 175, a site predicted to be deep in the protein, which led to a strong hyperpolarizing shift in I_{cot} and I_{leak}, was also only resolved at hyperpolarizing potentials (Fig. 2a). The changes in steady-state voltage dependence were reflected in the altered presteady-state charge distribution, which reports the result of partial reactions that precede P_i binding (Fig. 7). The unique behaviour of A175C (and A175C-S448C) may arise from the close proximity of site 175 to three residues (Ala190, Ala192 and Asp196) that we have previously shown to be critical determinants of both Na^+ interaction and electrogenicity in the mammalian NaPi-IIa isoforms [4, 39] (Fig. 1a).

These findings suggested that the residue at this site was an important determinant of voltage dependence and Na^+ interaction. In contrast, the weak effect of Cys substitutions at the external facing sites (155, 448) suggested that these sites were not critical determinants of Na^+ interactions. Moreover, our finding that we could partly restore the voltage dependence of A175C to the WT behaviour by the Ser-Cys substitution at 448 in the double mutant (A175C-S448C) supports the notion of the putative re-entrant domains forming an integral core region of the protein that defines its transport kinetics. Like A175C, A175C-S448C also showed a large I_{leak} at hyperpolarizing potentials (Fig. 2b), whereby its voltage dependence mirrored that of I_{cot}. This would be expected if the voltage dependence of the leak and cotransport modes was codetermined by common partial reactions in the kinetic scheme (Fig. 7).

We confirmed the effect of Cys substitutions on the voltage-dependent kinetics by numerical simulation of the cotransport cycle according to our kinetic scheme (see Appendix). Good agreement with experimental data for the substitution at 155 or 448 was obtained by altering the forward rate constant (k_{18}) of the empty carrier transition (1↔8). However, to simulate the effect of Cys substitution at 175, it was necessary to alter the rate constants (k_{12a}, k_{2a1}) that define the first Na^+ interaction from the external

solution (1↔2a; Table 3). The simulated steady-state *I–V* relationships (Fig. 8a) matched the shifts in voltage dependence of I_{cot} observed experimentally (Fig. 2a). According to the simulations, the effect of the Cys substitution at 175 was to increase the occupancy of state 8 (inward facing, empty carrier). This state became more favoured as the dissociation constant for the first Na^+ binding partial reaction was increased: to attain the same forward transport rate as the WT therefore required a stronger membrane hyperpolarisation as observed experimentally.

Simulations also gave valuable insight into the presteady-state behaviour of mutant A175C. By running them over a wider voltage range that would be experimentally impossible, we could show that the absence of *Q–V* saturation at negative test potentials simply reflected the limited range of hyperpolarizing potentials that could be applied. Thus, the charge movement measured was mainly contributed by the empty carrier: i.e. for A175C, Na^+-dependent partial reactions contributed significantly to overall charge movement only at very hyperpolarizing potentials. In contrast, for the WT (and S448C and S155C), the contributions to the *Q–V* from the empty carrier and electrogenic Na^+ interactions become merged within the experimental voltage range. Our fitting strategy using a single Boltzmann function therefore represents a compromise dictated by experimental and analytical constraints.

Cys modification alters transport mode and mobile charge movement

Using MTS reagents to effect in situ thiol modification of cysteines is a widely used method to identify functionally important sites and determine topological features of membrane transport proteins. We have applied this strategy extensively to SLC34 proteins [9, 10, 19, 20, 23, 24, 39]. After MTSET incubation, all constructs containing Cys448 showed suppression of I_{cot}, but I_{leak} remained detectable. We assume this behaviour resulted specifically from modification of Cys448 and that native cysteines of flNaPi-IIb are not involved, based on our finding that introduction of a Cys at the equivalent site in the Cys-reduced rat NaPi-IIa shows the same behaviour with respect to cotransport and leak [21]. We also observed a reduced mobile charge movement after thiol modification (Table 2), which we have previously interpreted as evidence of a reduction in the apparent electrical distance Na^+ must move to its binding site [43]. Despite this altered Na^+ interaction, modification of Cys448 provided us with a means to investigate the protein as it underwent transitions between a restricted number of states, thereby facilitating data interpretation.

In contrast to the behaviour of constructs with Cys448, the absence of significantly altered steady-state and presteady-state activity for A175C and S155C suggested that the introduced cysteines were either inaccessible from the external medium or, if modified, were functionally unimportant. Previous studies have shown that we can indeed label S155C [33, 42]. The lack of a functional change due to Cys modification of Cys155, which for MTSET would add both bulk and positive charge at this site, therefore suggested that the side chain at 155 is not itself a critical determinant of transport kinetics. On the other hand, Cys175 was most likely inaccessible from the external medium based on evidence obtained from the rat NaPi-IIa isoform with a Cys introduced at the equivalent site (A203C) [19].

Table 3 Rate constants for simulations using the 10-state model for electrogenic NaPi-IIb cotransport cycle

Forward rate constant		Backward rate constant	
k_{12a} [a,b] (M^{-1} s^{-1})		k_{2a1} [a] (s^{-1})	
WT	4.0×10^3 $\exp^{-0.4V/50}$	WT	8.0×10^2 $\exp^{0.4V/50}$
A175C	4.0×10^2 $\exp^{-0.4V/50}$	A175C	2.0×10^3 $\exp^{0.4V/50}$
S155C/S448C	2.0×10^3 $\exp^{-0.4V/50}$	S155C/S448C	4.0×10^2 $\exp^{0.4V/50}$
k_{2a2b} [b] (M^{-1} s^{-1})	6.0×10^3	k_{2b2a} (s^{-1})	2.0×10^2
k_{2b3} [b] (M^{-1} s^{-1})	4.0×10^6	k_{32b} (s^{-1})	8.0×10^3
k_{34} [b] (M^{-1} s^{-1})	4.0×10^5	k_{43} (s^{-1})	1.0×10^3
k_{87a} [a,b] (M^{-1} s^{-1})	1.0×10^3 $\exp^{-0.2V/50}$	k_{7a8} [a] (s^{-1})	1.0×10^3 $\exp^{0.2V/50}$
k_{7a7b} [b] (M^{-1} s^{-1})	1.0×10^3	k_{7b7a} (s^{-1})	1.0×10^3
k_{7b6} (M^{-1} s^{-1})	– [c]	k_{67b} (s^{-1})	1.0×10^3
k_{65} [b] (M^{-1} s^{-1})	1.0×10^5	k_{56} (s^{-1})	1.0×10^3
k_{45} (s^{-1})	25	k_{54} (s^{-1})	25 s^{-1}
k_{81} [a] (s^{-1})		k_{18} [a] (s^{-1})	
WT	1.0×10^2 $\exp^{-0.4V/50}$	WT	3.0×10^2 $\exp^{0.4V/50}$
A175C	1.0×10^2 $\exp^{-0.4V/50}$	A175C	3.0×10^2 $\exp^{0.4V/50}$
S155C/S448C	1.0×10^2 $\exp^{-0.4V/50}$	S155C/S448C	1.5×10^2 $\exp^{0.4V/50}$

[a] Voltage-dependent transitions were modelled using an Eyring barrier model assuming sharp, symmetrical barriers. We assume one net charge moves across the entire transmembrane electric field. The apparent valence of the empty carrier =−0.4; the charge movement contributed by a single Na^+ binding = 0.4 from the outside and =0.2 from the inside

[b] Pseudo first-order kinetics were assumed for all partial reactions involving substrate interaction

[c] Free parameter to satisfy the condition of microscopic reversibility required by the model

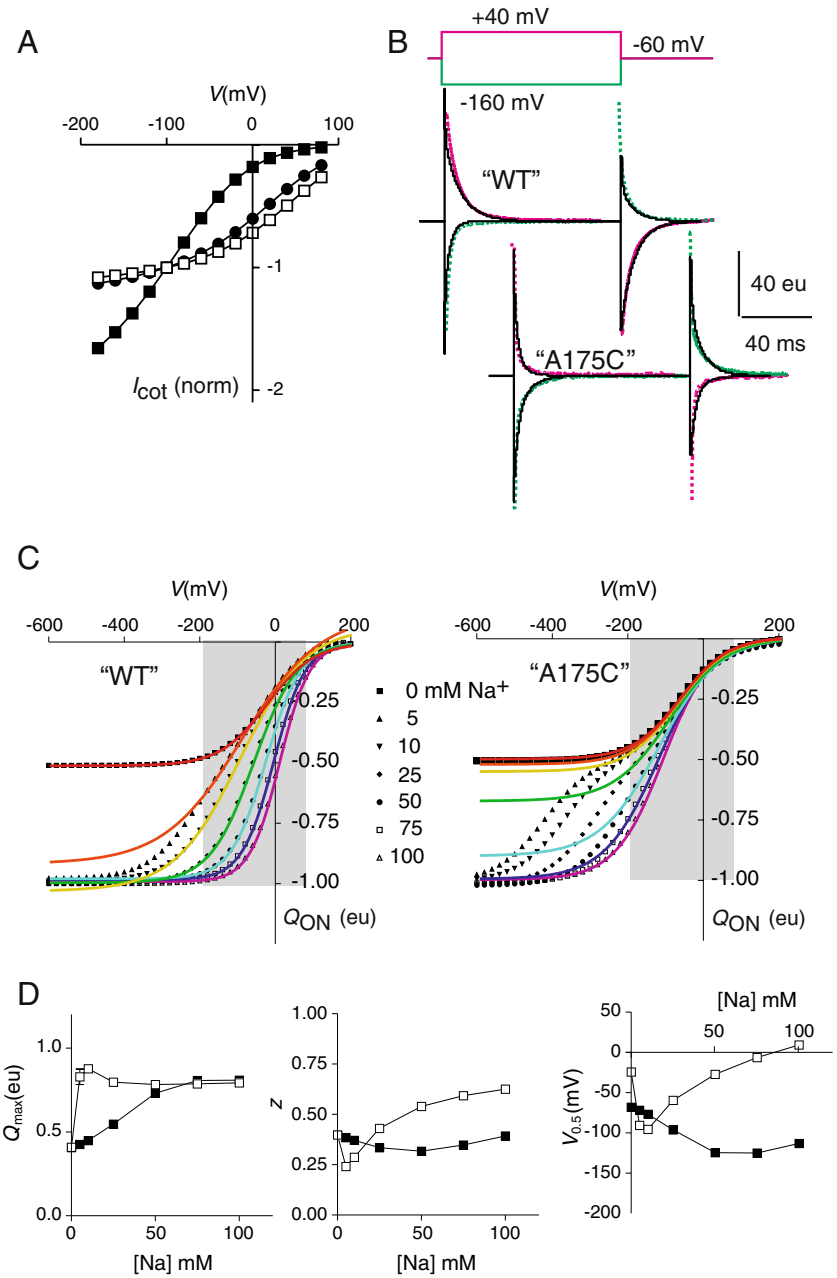

Fig. 8 Simulations predict voltage-dependent kinetics of single Cys substitutions. **a** Simulated voltage dependence of steady-state cotransport current (I_{cot}) given by Eq. 3, using parameters (Table 3) corresponding to the WT (*filled squares*), S448C or S155C (*open squares*) and A175C (*filled squares*). Data were normalised to I_{cot} at −100 mV to aid comparison with experimental data (Fig. 2a). **b** Presteady-state relaxations (*black traces*) obtained from Eq. 4 for the 100 mM Na^+ case in response to symmetrical voltage steps from −60 mV for WT and A175C. The NaPi-IIb-related presteady-state relaxations from Fig. 3b were scaled vertically and superimposed on the simulations. **c** *Q–V* as a function of [Na] obtained by integrating the simulated relaxations for the simulated WT and A175C. Note that for the experimental situation, the voltage window is restricted to the data points within the *shaded area* and therefore the fit with a single Boltzmann function (*coloured*, *continuous lines*) does not accurately describe the true charge distribution, especially for the simulated A175C. **d** Boltzmann parameters derived from fitting the shaded region in (**c**; −180 to +80 mV) with Eq. 2. WT (*empty squares*); A175C (*filled squares*). These data can be compared with the corresponding panels in Fig. 3b

From previous studies on the equivalent site to 448 in the rat NaPi-IIa protein (S460C), we concluded that after Cys modification of this site, the remaining NaPi-II electrogenic activity represents the leak mode (I_{leak}). This conclusion was based on the findings that: (1) ^{32}P uptake was suppressed after MTS treatment, indicating suppression of the cotransport mode; (2) the PFA response was the same before and after treatment, indicating that the leak mode was unchanged and (3) the response to P_i after MTS treatment was identical to the PFA response [20, 23], i.e. after MTS treatment $I_{cot}=0$, $I_{leak}=-I_{Pi}$. Na^+ and P_i interactions still occur, however, completion of the cotransport cycle is blocked. Under these conditions, state 3 with P_i bound is functionally equivalent to state 3* with PFA bound (Fig. 7). Of the three double mutants containing Cys448, the behaviour of A175C-S448C was consistent with this model: the condition $I_{cot}=0$ was reasonably valid over the range of test potentials applied (Fig. 2b). For S155C-S448C and A175S-S448C, resolution of the leak current was hampered by the presence of endogenous PFA and P_i-sensitive currents that partially masked the exogenous response, depending on the expression level. It was significant that the shifted voltage dependence of A175C was also observed in I_{leak} for A175C-S448C, before and after Cys modification, and in I_{Pi} after treatment. This supported the notion that the same elements in the protein

codetermine the voltage dependence of the leak and cotransport. However, we found that the magnitude of I_{leak} for A175C-S448C approximately doubled, in contrast to S448C, S155C-S448C and A175S-S448C, for which there was no resolvable change in I_{leak} after thiol modification. This suggested that Cys175 can modulate the phenotype of the S448C and hinted at a possible interaction between the first re-entrant domain and Cys448.

Promoting disulfide bridge formation: evidence for a state-dependent association of re-entrant domains

The strategy of chemical cross-linking between pairs of cysteines is a common approach to elucidate the functional association of helices and re-entrant regions in several membrane transport proteins (e.g. [6, 35, 37, 47]). Our cross-linking data provided compelling evidence that the association of the novel cysteines depended on the state of the protein: in 0Na, one or both cysteines in S155C-S448C were unable to cross link, whereas for A175C-S448C, cross-linking was more favourable, due to a different orientation or closer proximity of the novel cysteines. Three assumptions were implicit in the interpretation of our results: (1) disulfide bridge formation would have detectable functional consequences; (2) only the introduced cysteines were involved and (3) the disulfide bridges were intra- and not inter-molecular due to association between adjacent NaPi-II proteins or their oligomeric state. Although NaPi-II proteins are considered to be functional monomers [18], there is also indirect evidence that they may dimerise [15]. It is therefore possible that the oxidising treatment may have resulted in disulfide bridge formation between cysteines (novel or native) in adjacent monomers of dimers. That there was no loss of function after $CuPh_3$ incubation for the single Cys mutants, whether singly or co-expressed, confirmed that bridge formation occurred only between the introduced Cys in each monomer.

By assuming that the formation of a disulfide bridge in any monomer results in full inhibition of cotransport, our finding that the reduction of I_{Pi} for S155-S448C was greater than for A175C-S448C suggests that in the former construct, the two Cys are closer and therefore bridge formation was more favourable. This would accord with the predicted topology for TMD4 (Fig. 1a). Moreover, the suppression of the I_{Pi} was also dependent on the $CuPh_3$ incubation conditions, which further supported the notion that Na^+ effects a conformational change in the core region composed of the re-entrant domains and implicates them in Na^+ coordination. For $CuPh_3$ incubation of A175C-S448C in 0Na, the small loss of cotransport activity indicated that even in the absence of substrate, Cys175 and Cys448 may associate, albeit rarely. In contrast, for S155C-S448C loss of activity was only observed after incubation in 100Na. In this study, we only observed partial inhibition of the electrogenic response after $CuPh_3$ treatment. This suggested that disulfide bridge formation only occurred in a fraction of transporters and this was confirmed by re-exposure to MTSET, thereby indicating that at least one Cys of the pair was still available for thiol modification. The successful formation of a disulfide bridge is dependent on two rate constants: one associated with unproductive sulfhydryl oxidation of one cysteine and the other associated with bridge formation itself [5]. The amount of inhibition at the end of the $CuPh_3$ incubation reaction may then be taken as a measure of the probability of finding the respective Cys within a distance of 15.2 Å of one another [5].

Finally, we also found no significant change in the total mobile charge movement, which contrasts with the effect of thiol modification of the introduced cysteines. This suggested that the cross-linking had neither immobilised the empty carrier nor interfered with the ability of Na ions to enter the electric field.

Evidence for substrate- and voltage-dependent interactions between re-entrant domains from voltage clamp fluorometry

In contrast to presteady-state relaxations, which reflect global conformational changes that involve the concerted movement of perhaps many charges as the protein undergoes transitions between states in response to rapid changes in membrane potential, VCF offers a means of detecting local conformational changes in the microenvironment of a fluorophore [7, 26, 27, 30, 31, 42, 43]. The difference in the voltage-dependent parameters obtained by the two methods is seen by comparing $V_{0.5}$ and z obtained from the Q–V analysis (after MTSET treatment) and fluorescence (Table 2).

We compared the changes in fluorescent intensity (ΔF) induced by voltage steps under three superfusion conditions that allow investigation of the empty carrier alone and the carrier with one or both substrates present. The following interpretations were made:

– *ΔF reported by the labelled single mutants depends on the site of Cys substitution*. For labelled S448C, only the leak mode operates, and any ΔF should only result from transitions involved in the leak cycle (Fig. 7). For S448C, it is significant that no ΔF was detected in 0Na (empty carrier) [43]. In contrast, the labelled S155C reports ΔF for the three superfusion conditions with different magnitude and voltage dependences [42]: this suggested that the microenvironment of the fluorophore at site 155 was influenced by molecular rearrangements associated with partial reactions between all states in the transport cycle. As labelling Cys155 only marginally affected the electrogenic properties of S155C (Fig. 2a and [42]), we assume that changes in this

fluorophore's microenvironment reflect conformational changes of the normal transport cycle. In contrast, for A175C, consistent with lack of any change in electrogenic kinetics observed after MTSET exposure, we also observed no ΔF. We therefore conclude that this site must be either poorly accessible or if labelled, the added bulk of the MTS reagent does not alter the transport properties. The latter seems unlikely considering the change the Ala-Cys substitution alone had on the voltage dependence. Moreover, it was previously shown for the equivalent site (Ala203) in the rat NaPi-IIa isoform that it is poorly accessible from the external medium [20].

- *The side chain at site 175 in re-entrant domain 1 influences the microenvironment of the fluorophore at 448*. For S448C, A175C-S448C and A175S-S448C the protein operates in the leak mode. In 0Na, labelled Cys448 does not respond to potential in 0Na, therefore the ΔF measured from A175C-S448C suggested that Cys175 had altered the microenvironment of the labelled Cys448 such that it responded to voltage-dependent reorientation of the empty carrier. Alternatively, if Cys175 were also labelled, ΔF would reflect changes in the microenvironment of its fluorophore. Although we favour the former scenario, we are unable to distinguish between these two possibilities from the present data. When the non-polar Ala175 was substituted with a polar Ser, the labelled Cys448 reported no ΔF for 0Na and in 100Na, the ΔF–V that lay between that of the S448C and the A175C-S448C. This behaviour underscores the importance of the side chain at this site in determining voltage dependence. If both substrates were present, ΔF reported by the A175S-S448C was very similar to that for S448C alone, whereas with a Cys at 175, no ΔF was reported. These findings suggested that the structural changes induced by altering the side chain at 175 can influence how the fluorophore at 448 responds to its microenvironment.
- *Cys448 influences the microenvironment of the fluorophore at 155 in re-entrant domain 1*. For S155C-S448C, ΔF in 0Na was nearly identical to that of labelled S155C and as labelled S448C show no ΔF in 0Na, this suggested that ΔF from S155C-S448C arises only from changes to the microenvironment of the fluorophore at Cys-155. In 100Na, S155C and S448C report ΔF, but with significantly different voltage dependences (Table 2). According to our kinetic scheme (Fig. 7), ΔF obtained from labelled S155C should reflect contributions from Na^+ binding and the empty carrier, whereas the labelled S448C only reports Na^+ interactions. Therefore, if both cysteines were labelled in S155C-S448C, we would predict that its ΔF–V would be the combined response of the two single mutants under the same conditions. Instead, we observed a ΔF–V with a weak voltage dependence, similar to ΔF–V for S448C in 100Na (z^F in 100Na reduced to 0.2, Table 2), and also when both substrates were present. These findings suggest that Cys448 altered the microenvironment of the fluorophore at Cys155, but conditional on the presence of one or both substrates.

Without more structural information it is not possible to interpret the ΔF–V data in terms of specific local molecular rearrangements in the environment of the fluorophores, nevertheless our data demonstrate how a side chain substituted at a functionally critical site in one domain can affect the change in fluorescence intensity reported by a labelled Cys in the opposed domain. Moreover, they show how the presence or absence of substrate can determine the structural rearrangements that occur in different parts of the protein.

Conclusions

We have identified a site in the first putative re-entrant domain that is a critical determinant of voltage dependence and Na^+ interaction. Moreover, we provide evidence from fluorometry and cross-linking that this site can interact with one in the second putative re-entrant domain. Our findings lend functional support to the importance of the *trans* repeat architecture in cation-coupled cotransporters.

Acknowledgments We gratefully acknowledge Eva Hänsenberger for oocyte preparation and Dr. Leila Virkki for generating the A175C-S448C mutant. This work was supported by the Swiss National Science Foundation grants to HM and ICF and from the Alfred Benzon Foundation (Denmark) to AKM.

Appendix: Simulations using a ten-state kinetic model for the cotransport cycle

The set of differential equations that describes the cotransport cycle according to the ten-state kinetic scheme (Fig. 7) was solved numerically for the state occupancies, steady-state current and presteady-state charge movement (e.g. [9, 32]). For these simulations, we ignored the leak pathway and we assumed that transition 4–5 (translocation of fully loaded carrier) was electroneutral and that the apparent equivalent charge of the empty carrier was −1. Under these conditions, transition 1–8 is the only one that involves net transmembrane charge movement and therefore the steady-state P_i-induced current for N transporters given by:

$$I_{\mathrm{cot}} = N z_t (k_{18} X_1 - k_{81} X_8) \quad (3)$$

where z_t is the net translocated charge per cotransport cycle (z_t=1) and where X_n is the occupancy of state n and k_{ij} is the transition rate from state i to state j.

The pre-steady-state current per cotransporter molecule is given by:

$$I_{pss} = -e(\alpha'(k_{12}X_1 - k_{21}X_2) - d(k_{18}X_1 - k_{81}X_8) + \alpha''(k_{78}X_7 - k_{87}X_8)) \quad (4)$$

where the equivalent charge of −1 of the empty carrier moves an equivalent electrical distance δ through the membrane and for the Na^+ binding transitions (1–2a, 8–7) also involve movement of +1 charge through equivalent electrical distances α' and α'', respectively. Thus, one net charge moves across the whole of the membrane electric field and $1=\alpha'+\alpha''+\delta$. The expressions for the transition rates for electrogenic transitions were modelled according to Eyring transition state theory in which the apparent charge moves over a sharp symmetrical barrier. The forward and backward rate constants for voltage-dependent transitions are given by:

$$k_{18} = k_{18}^{o} \exp(\delta V/2kT) \quad (5a)$$

$$k_{81} = k_{81}^{o} \exp(-\delta V/2kT) \quad (5b)$$

$$k_{12} = [Na]_o k_{12}^{o} \exp(-\alpha' V/2kT) \quad (5c)$$

$$k_{21} = k_{21}^{o} \exp(\alpha' V/2kT) \quad (5d)$$

$$k_{87a} = [Na]_i k_{87a}^{o} \exp(-\alpha'' V/2kT) \quad (5e)$$

$$k_{7a8} = k_{7a8}^{o} \exp(\alpha'' V/2kT) \quad (5f)$$

where k_{ij}^{o} is the rate constant for transition ij at V=0 and $[Na]_{o/i}$ are the external and internal concentrations of Na^+ (mole/l), respectively. To satisfy microscopic reversibility, k_{7b6} was defined in terms of the other rate constants:

$$k_{7b6} = \frac{k_{67b}^{o} k_{7b7a}^{o} k_{7a8}^{o} k_{81}^{o} k_{12a}^{o} k_{2a2b}^{o} k_{2b3}^{o} k_{34}^{o} k_{45}^{o} k_{56}^{o}}{k_{65}^{o} k_{54}^{o} k_{43}^{o} k_{32b}^{o} k_{2b2a}^{o} k_{2a1}^{o} k_{18}^{o} k_{87a} k_{7a7b}} \quad (6)$$

We began with a set of rate constants and intrinsic charges that described the steady-state and pre-steady-state behaviour of the WT (Table 3) and adjusted the rates to give a reasonable match by eye to the experimental findings. The simulated steady-state I–V relationships (Fig. 8a) predicted the shifts in voltage dependence of I_{cot} observed experimentally (Fig. 2a). The simulations also established that $K_{0.5}^{Pi}$ was relatively insensitive to the changes in the rate constants, whereas $K_{0.5}^{Na}$ increased for the simulated A175C case, as found experimentally (Table 1; not shown).

The presteady-state relaxations in the absence of P_i for the simulated WT and A175C case also recapitulated the experimental data (Fig. 8b). The corresponding Q–V data for varying $[Na^+]$ gave different steady-state charge distributions for the simulated WT and A175C cases (Fig. 8c). The Q–V data for the simulated A175C revealed two distinct Boltzmann distributions, which become more apparent at low $[Na^+]$ by extending the voltage range in the hyperpolarizing direction. If the simulated data were fit with a single Boltzmann function within the experimental voltage range, the predicted Boltzmann parameters (Fig. 8d) showed qualitatively the same behaviour as the experimental data (Fig. 3c). In particular, $V_{0.5}$ predicted by the single Boltzmann fit to the simulated Q–V data became more negative with increasing $[Na^+]$, and reached a plateau close to 100 mM (Fig. 8c), which was in agreement with the Boltzmann analysis of the experimental data (Fig. 3b).

References

1. Abramson J, Wright EM (2009) Structure and function of Na(+)-symporters with inverted repeats. Curr Opin Struct Biol 19 (4):425–432. doi:10.1016/j.sbi.2009.06.002
2. Abramson JSI, Kasho V, Verner G, Kaback HR, Iwata S (2003) Structure and mechanism of the lactose permease of *Escherichia coli*. Science 301(5633):610–615
3. Andrini O, Ghezzi C, Murer H, Forster IC (2008) The leak mode of type II Na(+)-P(i) cotransporters. Channels (Austin) 2(5):346–357
4. Bacconi A, Virkki LV, Biber J, Murer H, Forster IC (2005) Renouncing electrogenicity is not free of charge: switching on electrogenicity in a Na^+-coupled phosphate cotransporter. Proc Natl Acad Sci U S A 102:12606–12611
5. Careaga CL, Falke JJ (1992) Thermal motions of surface alpha-helices in the D-galactose chemosensory receptor. Detection by disulfide trapping. J Mol Biol 226(4):1219–1235
6. Castagna M, Soragna A, Mari SA, Santacroce M, Bette S, Mandela PG, Rudnick G, Peres A, Sacchi VF (2007) Interaction between lysine 102 and aspartate 338 in the insect amino acid cotransporter KAAT1. Am J Physiol Cell Physiol 293(4):C1286–C1295
7. Cha A, Bezanilla F (1998) Structural implications of fluorescence quenching in the Shaker K+ channel. J Gen Physiol 112(4):391–408
8. Dutzler R, Campbell EB, Cadene M, Chait BT, MacKinnon R (2002) X-ray structure of a ClC chloride channel at 3.0 A reveals the molecular basis of anion selectivity. Nature 415(6869):287–294
9. Ehnes C, Forster IC, Bacconi A, Kohler K, Biber J, Murer H (2004) Structure–function relations of the first and fourth extracellular linkers of the type IIa Na^+/P_i cotransporter: II. Substrate interaction and voltage dependency of two functionally important sites. J Gen Physiol 124:489–503
10. Ehnes C, Forster IC, Kohler K, Bacconi A, Stange G, Biber J, Murer H (2004) Structure–function relations of the first and fourth

predicted extracellular linkers of the type IIa Na^+/Pi cotransporter: I. Cysteine scanning mutagenesis. J Gen Physiol 124(5):475–488
11. Forrest LR, Rudnick G (2009) The rocking bundle: a mechanism for ion-coupled solute flux by symmetrical transporters. Physiology (Bethesda) 24:377–386
12. Forster I, Hernando N, Biber J, Murer H (1998) The voltage dependence of a cloned mammalian renal type II Na^+/P_i cotransporter (NaPi-2). J Gen Physiol 112(1):1–18
13. Forster IC, Wagner CA, Busch AE, Lang F, Biber J, Hernando N, Murer H, Werner A (1997) Electrophysiological characterization of the flounder type II Na^+/P_i cotransporter (NaPi-5) expressed in *Xenopus laevis* oocytes. J Membr Biol 160(1):9–25
14. Ghezzi C, Murer H, Forster IC (2009) Substrate interactions of the electroneutral Na+-coupled inorganic phosphate cotransporter (NaPi-IIc). J Physiol 587(Pt 17):4293–4307
15. Gisler SM, Kittanakom S, Fuster D, Wong V, Bertic M, Radanovic T, Hall RA, Murer H, Biber J, Markovich D, Moe OW, Stagljar I (2008) Monitoring protein–protein interactions between the mammalian integral membrane transporters and PDZ-interacting partners using a modified split-ubiquitin membrane yeast two-hybrid system. Mol Cell Proteomics 7(7):1362–1377
16. Hilfiker H, Hattenhauer O, Traebert M, Forster I, Murer H, Biber J (1998) Characterization of a murine type II sodium-phosphate cotransporter expressed in mammalian small intestine. Proc Natl Acad Sci U S A 95(24):14564–14569
17. Huang XMM (1991) A time-efficient, linear-space local similarity algorithm. Adv Appl Math 12:337–357
18. Kohler K, Forster IC, Lambert G, Biber J, Murer H (2000) The functional unit of the renal type IIa Na+/Pi cotransporter is a monomer. J Biol Chem 275(34):26113–26120
19. Kohler K, Forster IC, Stange G, Biber J, Murer H (2002) Identification of functionally important sites in the first intracellular loop of the NaPi-IIa cotransporter. Am J Physiol 282(4):F687–F696
20. Kohler K, Forster IC, Stange G, Biber J, Murer H (2002) Transport function of the renal type IIa Na^+/P_i cotransporter is codetermined by residues in two opposing linker regions. J Gen Physiol 120:693–703
21. Kohler K, Forster IC, Stange G, Biber J, Murer H (2003) Essential cysteine residues of the type IIa Na^+/P_i cotransporter. Pflügers Arch Eur J Physiol 446(2):203–210
22. Krishnamurthy HPC, Gouaux E (2009) Unlocking the molecular secrets of sodium-coupled transporters. Nature 459(7245):347–355
23. Lambert G, Forster IC, Stange G, Biber J, Murer H (1999) Properties of the mutant Ser-460-Cys implicate this site in a functionally important region of the type IIa Na^+/P_i cotransporter protein. J Gen Physiol 114(5):637–652
24. Lambert G, Forster IC, Stange G, Kohler K, Biber J, Murer H (2001) Cysteine mutagenesis reveals novel structure–function features within the predicted third extracellular loop of the type IIa Na^+/P_i cotransporter. J Gen Physiol 117(6):533–546
25. Larkin MA, Blackshields G, Brown NP, Chenna R, McGettigan PA, McWilliam H, Valentin F, Wallace IM, Wilm A, Lopez R, Thompson JD, Gibson TJ, Higgins DG (2007) ClustalW and ClustalX version 2. Bioinformatics 23(21):2947–2948
26. Larsson HP, Tzingounis AV, Koch HP, Kavanaugh MP (2004) Fluorometric measurements of conformational changes in glutamate transporters. Proc Natl Acad Sci U S A 101(11):3951–3956
27. Li M, Lester HA (2002) Early fluorescence signals detect transitions at mammalian serotonin transporters. Biophys J 83(1):206–218
28. Lolkema JS, Slotboom DJ (2003) Classification of 29 families of secondary transport proteins into a single structural class using hydropathy profile analysis. J Mol Biol 327(5):901–909
29. Lolkema JS, Slotboom DJ (2008) The major amino acid transporter superfamily has a similar core structure as Na+-galactose and Na+-leucine transporters. Mol Membr Biol 25(6–7):567–570
30. Loo DD, Hirayama BA, Gallardo EM, Lam JT, Turk E, Wright EM (1998) Conformational changes couple Na+ and glucose transport. Proc Natl Acad Sci U S A 95(13):7789–7794
31. Meinild AK, Hirayama BA, Wright EM, Loo DD (2002) Fluorescence studies of ligand-induced conformational changes of the Na^+/glucose cotransporter. Biochemistry 41(4):1250–1258
32. Parent L, Supplisson S, Loo DD, Wright EM (1992) Electrogenic properties of the cloned Na+/glucose cotransporter: II. A transport model under nonrapid equilibrium conditions.[erratum appears in J Membr Biol 1992 Nov;130(2):203]. J Membr Biol 125(1):63–79
33. Radanovic T, Gisler SM, Biber J, Murer H (2006) Topology of the type IIa Na+/P(i) cotransporter. J Membr Biol 212(1):41–49. doi:10.1007/s00232-006-0033-2
34. Ravera S, Virkki LV, Murer H, Forster IC (2007) Deciphering PiT transport kinetics and substrate specificity using electrophysiology and flux measurements. American Journal of Physiology-Cell Physiology 293(2):C606–C620
35. Ryan RM, Mitrovic AD, Vandenberg RJ (2004) The chloride permeation pathway of a glutamate transporter and its proximity to the glutamate translocation pathway. J Biol Chem 279 (20):20742–20751
36. Screpanti E, Hunte C (2007) Discontinuous membrane helices in transport proteins and their correlation with function. J Struct Biol 159(2):261–267. doi:S1047-8477(07)00031-7
37. Tao Z, Zhang YW, Agyiri A, Rudnick G (2009) Ligand effects on cross-linking support a conformational mechanism for serotonin transport. J Biol Chem 284(49):33807–33814
38. Virkki LV, Biber J, Murer H, Forster IC (2007) Phosphate transporters: a tale of two solute carrier families. Am J Physiol Renal Physiol 293(3):F643–F654
39. Virkki LV, Forster IC, Bacconi A, Biber J, Murer H (2005) Functionally important residues in the predicted 3rd transmembrane domain of the type IIa sodium-phosphate co-transporter (NaPi-IIa). J Membr Biol 206(3):227–238
40. Virkki LV, Forster IC, Biber J, Murer H (2005) Substrate interactions in the human type IIa sodium-phosphate cotransporter (NaPi-IIa). Am J Physiol 288:F969–F981
41. Virkki LV, Forster IC, Hernando N, Biber J, Murer H (2003) Functional characterization of two naturally occurring mutations in the human sodium-phosphate cotransporter type IIa. J Bone Miner Res 18(12):2135–2141
42. Virkki LV, Murer H, Forster IC (2006) Mapping conformational changes of the type IIb Na^+/P_i cotransporter by voltage clamp fluorometry. J Biol Chem 281:28837–28849
43. Virkki LV, Murer H, Forster IC (2006) Voltage clamp fluorometric measurements on a type II Na^+-coupled P_i cotransporter: shedding light on substrate binding order. J Gen Physiol 127:539–555
44. Werner A, Kinne RK (2001) Evolution of the Na-P_i cotransport systems. Am J Physiol 280(2):R301–R312
45. Yamashita A, Singh SK, Kawate T, Jin Y, Gouaux E (2005) Crystal structure of a bacterial homologue of Na+/Cl–dependent neurotransmitter transporters. Nature 437(7056):215–223
46. Yernool DBO, Jin Y, Gouaux E (2004) Structure of a glutamate transporter homologue from *Pyrococcus horikoshii*. Nature 431 (7010):811–818
47. Zomot E, Zhou Y, Kanner BI (2005) Proximity of transmembrane domains 1 and 3 of the gamma-aminobutyric acid transporter GAT-1 inferred from paired cysteine mutagenesis. J Biol Chem 280(27):25512–25516